Applied Clay Science 121–122 (2016) 127–136

Contents lists available at ScienceDirect

Applied Clay Science

journal homepage: www.elsevier.com/locate/clay

Improved photocatalytic activity of SnO_2–ZnAl LDH prepared by one step Sn^{4+} incorporation

G. Mendoza-Damián [a,*], F. Tzompantzi [a], A. Mantilla [b], R. Pérez-Hernández [c], A. Hernández-Gordillo [d,1]

[a] Depto. de Química, Área de Catálisis, Universidad Autónoma Metropolitana — Iztapalapa, Av. San Rafael Atlixco No. 189, México, D.F. 09340, México
[b] Instituto Politécnico Nacional CICATA—Legaria, Legaria No. 694, México, D.F. 11500, Mexico
[c] Instituto Nacional de Investigaciones Nucleares, Carretera México-Toluca S/N La Marquesa, Ocoyoacac, Edo. México C.P. 52750, Mexico
[d] Instituto de Investigaciones en Materiales, Universidad Nacional Autónoma de México, Circuito Exterior SN, Ciudad Universitaria, Coyoacán, C.P. 04510 México, D.F., Mexico

ARTICLE INFO

Article history:
Received 7 August 2015
Received in revised form 1 December 2015
Accepted 8 December 2015
Available online 15 December 2015

Keywords:
SnO_2–ZnAl LDH
SnO_2 oxide
Phenol photo-degradation
SnO_2 impregnated

ABSTRACT

SnO_2–ZnAl LDH with a molar ratio Zn/(Al + Sn) 3/1 (Sn^{4+} contents 0.1–0.4 mol%) were prepared in one step by the co-precipitation method. The ZnAl LDH intercalated with carbonate ions and the composite of ZnAl LDH formed together with SnO_2 were characterized by XRD, SEM, HRTEM and complementary spectroscopies such as FTIR, XPS and UV–Vis. The EDX and AAS was performed for the compositional analysis. The effect of the Sn^{4+} content on the opto-electronic properties of the dried SnO_2–ZnAl LDH composites were evaluated on the phenol photodegradation under UV light irradiation. The mineralization degree of the photocatalysts was determined after 2 h of reaction by TOC analysis. The SnO_2–ZnAl LDH composites that showed the highest photocatalytic activity were compared with ZnAl LDH sample impregnated with Sn^{4+} cations. The effect of the presence of the $Zn_5(CO_3)_2(OH)_6$ as precursor for the formation of the ZnAl LDH as well as the methodology of synthesis on the photocatalytic properties of the composites were studied. A possible mechanism of the •OH radical formation and electron–hole charge separation in the improvement photocatalytic reaction were discussed.

1. Introduction

Nowadays, the continuous intensification of the environmental pollution has increased the interest on the progress of Advanced Oxidation Processes (AOP) (Herrmann, 2010a, 2010b). In this field, the development of new materials whose adequate electronic properties allows the complete oxidation and mineralization of harmful organic compounds such as phenol using UV or visible light irradiation is in particular an important goal of the AOP. Although TiO_2 and ZnO semiconductors are the most known photocatalysts reported in the literature for the AOP (Sobczynski et al., 2004; Guo et al., 2006; Parida et al., 2010), many efforts have been focused on exploring innovative alternatives, particularly the development of effective composites for the photooxidation reactions. In this way it has been recently reported the use of layered double hydroxides (LDH) as photocatalysts for environmental remediation (Cavani et al., 1991; Bravo-Suárez et al., 2004, Xiang et al., 2014) a special attention has been devoted to ZnAl–La (Tzompantzi et al., 2011) and Zn/(Al, Fe, Cr, Co or Sn) (Seftel et al., 2008a, 2008b; Zhao et al., 2011; Mohapatra and Parida, 2012; Parida and Mohapatra, 2012, He et al., 2015a) composites. These solids are not traditional semiconductors and the charge transfer from oxygen atoms to the metal cations (M^{2+} or M^{3+}) is reported as the responsible of its photoactivity (Mohapatra and Parida, 2012). The charge transfer leads to an effective charge separation of the electron–hole pairs, where the holes react with water to form •OH radicals, whereas the electrons react with the dissolved oxygen to form superoxide radicals (O_2^{-*}). These radicals are well known as the oxidizing species that carry out the photodegradation of phenolic compounds (Tzompantzi et al., 2011; Zhao et al., 2011) as well as azo dyes (Rhodamine B, Methyl Violet, and Methyl Orange) on LDH (Seftel et al., 2008a, 2008b; Mohapatra and Parida, 2012; Parida and Mohapatra, 2012). In most of the cases, the LDH are annealed in the intervals from 300 to 600 °C to form mixed metal oxides (MMOs) like ZnO–$ZnAl_2O_4$ (Zhao et al., 2011), MgO/ZnO/In_2O_3 (Xiang et al., 2013) or ZnO/SnO_2 (Seftel et al., 2008b), where the electron–hole recombination is decreased and its photoactivity improved. Layered double hydroxides (LDH) are materials obtained from a partial substitution of divalent (M^{2+}) by trivalent (M^{3+}) cations in a Brucite structure ($Mg(OH)_2$), adopting the formula $[M^{2+}{}_{1-x}M^{3+}{}_x(OH)_2]^{x+}[A^{n-}{}_{x/n}]\cdot nH_2O$, where A^{n-} are the compensation anions like NO_3^-, SO_4^{2-}, Cl^-, CO_3^{2-}, and OH^- that are intercalated in the interlayer space (Cavani et al., 1991; Bravo-Suárez et al., 2004). However, it has been reported that is possible to synthesize LDH with insertion of tetravalent (M^{4+}) cations (Das and Samal, 2004). The insertion of Ti^{4+} cations into ZnAl (Sahu et al., 2013) and MgAl LDH structures (Mendoza-Damián et al., 2013), as well as Sn^{4+} cations into MgAl (Velu et al., 1999; Tong et al., 2010) and ZnAl LDH (Seftel et al.,

* Corresponding author.
E-mail address: zyanya_8@hotmail.com (G. Mendoza-Damián).
[1] CONACYT Research Fellow.

http://dx.doi.org/10.1016/j.clay.2015.12.007
0169-1317/

2008c) have successfully achieved, generating ternary LDH where the hydroxylation, textural, morphological and opto-electronic properties of the annealed materials are very different to the binary LDH. In our knowledge, ZnAl LDH structures intercalated with carbonate ions and modified with Sn^{4+} cations have not been studied for the photocatalytic degradation of organic compounds. In this way, the purpose of the present work is to study the effect of SnO_2 content on the $[Zn_3Al(OH)_8]^{2+}[(-CO_3)^{2-}]\cdot nH_2O$ LDH photocatalytic properties prepared in one step. For comparison purpose a SnO_2–ZnAl LDH sample was synthesized by impregnation method (0.3 mol% of Sn^{4+}). The synthesized composites were characterized by X-ray diffraction (XRD), UV–Vis diffuse reflectance (UV–Vis–DR), infrared (FTIR) and X-ray photoelectron (XPS) spectroscopies, scanning electron microscopy (SEM) and high resolution-TEM (HRTEM), electron dispersed X-ray (EDX) and atomic absorption spectroscopy (AAS). The photocatalytic activity of these composites was studied in the phenol photodegradation with UV irradiation and the mineralization was followed by total organic carbon (TOC) analysis. The •OH radical generation was determined for the selected composite by the fluorescence of hydroxylated terephthalic acid. The possible photodegradation mechanism of phenol was discussed.

2. Experimental

2.1. Synthesis of SnO_2–ZnAl composites LDH

SnO_2–ZnAl LDH were synthesized in one step by the co-precipitation method using $Zn(NO_3)_2{:}6H_2O$, $Al(NO_3)_3{:}9H_2O$ (Fermont, 99%) and $SnCl_4{:}5H_2O$ (Sigma Aldrich, 98%) solutions as metallic precursors. The amount of the solutions containing zinc or aluminum was adjusted to obtain a constant $Zn / (Al_{1-x} + Sn_x) = 3/1$ molar ratio and a variable Sn_x content (0.1, 0.2, 0.3 and 0.4 mol%). The mixed solution was heated at 70 °C under continuous stirring during 4 h, and then an aqueous solution of urea (NH_2CONH_2) with a molar ratio NO_3^-/urea = 2 was added in order to carry out the hydrolysis at pH 9.0 ± 0.5. The mixed solution was then kept under reflux at 95 °C during 36 h. The precipitated solid was filtered and washed with distilled water at 90 °C. Finally the obtained solids were dried at 100 °C overnight. The labeling of different LDH composites was referred as ZA–SnX, where the X represents the Sn^{4+} content. In separate reactions, ZnAl LDH and SnO_2 bulk were synthesized in a similar way, following the above procedure and labeling as ZA and SnO_2, respectively.

2.2. Synthesis of SnO_2–ZnAl^{Imp} LDH

First one, the metallic precursors of Zn and Al were dissolved in aqueous solution, then the mixed solution was heated to 70 °C under continuous stirring during 4 h, and an aqueous solution of urea was added in order to carry out the hydrolysis at pH 9.0 ± 0.5. After 6 h once the ZnAl LDH is formed, appropriate amount of a $SnCl_4$ solution was added (0.3 mol%), and then it was put under reflux at 95 °C for 36 h. The sample was filtered, washed, dried and labeled as ZA–Sn3^{Imp}.

2.3. Characterization

X-ray powder diffraction of the LDH was obtained at room temperature using a Bruker D2 PASHER with a lynx eye detector diffractometer. Diffraction patterns were acquired between 8 and 65°, 2θ, with a step of $0.01°s^{-1}$, and using a CuKα source (λ = 0.154 nm). The identification of the diffraction peaks from the XRD patterns was carried out using the JCPDS database. The lattice parameters were estimated using the Bragg Law. The characteristic vibrations of the materials were determined by using a FTIR Affinity-1 Shimadzu spectrophotometer equipped with an attenuate total reflectance ATR accessory. Diffuse reflectance UV–Vis spectra of the samples were analyzed from 190 to 800 nm by using a VARIAN Cary-100 spectrophotometer, equipment with integration sphere and using $BaSO_4$ as reference blank. The morphological characterization of the selected LDH samples was performed in a low vacuum scanning electron microscope (LVSEM) JEOL JSM-6610LV at 20 kV, equipped with an energy dispersive X-ray spectroscope (EDX, INCAX-act-Oxford). The absorption atomic spectrometry-flame of Al, Sn and Zn, were determined using a Perkin Elmer AANALYST-700 atomic absorption spectrometer. The detection of the metals was performed at specific wavelengths for each element, Al: 396.1 nm, Sn: 284.0 nm, and Zn: 213.9 nm, using monoelemental hollow-cathode lamps. Three calibration curves were performed with 5 different concentrations of each element. The linear correlation coefficient was higher than 0.997 in all the cases.

The X-ray photoelectron analysis (XPS) was carried out using a Thermo K-Alpha photoelectron spectrometer equipped with a monochromatic Al X-ray source (1486.6 eV). The samples were deposited on a conducting scotch tape and studied without any pretreatment. The spot size of the XPS source on the sample was 400 μm. The base pressure of the analysis chamber was 10^{-9} mbar, a beam of Ar ions was applied to the samples to reduce the electrostatic charges, it increased the pressure up to 10^{-7} mbar in which the analysis was performed. The samples were located in Al tapes on stainless steel sample holders, which remained in a pre-analysis chamber for approximately 1 h at 10^{-3} mbar before entering the analysis chamber. The step energy of the survey mode was 1 eV, but in the C1s, O1s, Al2p, Zn2p and Sn3d orbital scans, the energy step was adjusted to obtain approximately 600 points per each distribution. This means energy steps between 0.09 and 0.03 eV, depending on the element and the energetic region. The $Au4f_{7/2}$ energy peak at 84.0 ± 0.1 eV and the $Ag3d_{5/2}$ XPS line position (368.22 eV) are used to calibrate the BE scale of the spectrometer. The high resolution electron microscopy (HRTEM) was performed in a JEOL 2100F electron microscope, fitted with a GATAN double tilt goniometer stage (±22°). Further the FFT of HRTEM image analysis was performed with Digital Micrograph software program.

2.4. Photocatalytic evaluations

The photocatalytic activity of the SnO_2–ZnAl LDH composites was evaluated in the photodegradation of phenol in aqueous solution. A solution with 40 ppm concentration (4.2×10^{-4} mol/L) of phenol in deionized water was prepared and bubbled in airflow at 1 mL s^{-1} for 12 h. Then 200 mL of the aerated solution and 0.2 g (1 g/L) of the photocatalyst powder were put into a batch-type built-in-house glass reactor (250 mL). The reaction mixture was stirred at 700 rpm under airflow (1 mL s^{-1}) for 1 h under dark and then an aliquot of the suspension was taken in order to determine the adsorption phenomena. Afterwards, the suspension was irradiated with an UV light Pen-Ray UV power lamp with a wavelength of 254 nm (I_0 = 4.4 mW cm^{-2}), which was immersed in the solution and protected by a quartz tube. The concentration of phenol was followed by measuring its maximum absorption band (λ = 269 nm) using a VARIAN CARY 100 spectrophotometer. Aliquots of the irradiated solution at short intervals were taken during 120–300 min of reaction. Additionally, phenol photodegradation was carried out in the absence of photocatalyst (photolysis). In these experimental conditions, the photocatalyst absorb 27 times more UV light than the phenol, due to that the optical density of the phenol at 254 nm is 0.25 (at 40 ppm) and for the photocatalyst is 6.8 (for 1 g/L).

The amount of total organic carbon present in the irradiated solution was determined with a TOC-V CSH/CSN Shimadzu Analyzer. The kinetic parameters (k and $t_{1/2}$) were obtained considering a pseudo first order reaction.

2.5. •OH radical determination

Fluorescence spectra of 2-hydroxyterephthalic acid were measured on a SCINCO fluorescence spectrometer FS-2. The •OH radical generated by the material semiconductor in absence of the phenol was evaluated

by using the following procedure: terephthalic acid (TA) (5×10^{-4} M) was dissolved in a water/NaOH solution (2×10^{-3} M). Then 200 mg of photocatalysts was added and the suspension was stirred for 60 min under dark condition. After it was irradiated by a UV light Pen-Ray lamp with a wavelength of 254 nm ($I_0 = 4.4$ mW cm^{-2}), during 10 min, and aliquots were taken each 2 min. The fluorescence emission spectra of the irradiated solution were analyzed by PL (excited at 320 nm).

3. Results and discussion

3.1. Structural analyses

The XRD patterns of the ZnAl LDH and SnO_2–ZnAl LDH composites, Fig. 1, showed reflection of the planes (003), (006), (012), (015), (018), (110), and (113), which are characteristics of the typical ZnAl layered double hydroxide (LDH) structures with intercalated carbonate ions (Ahmed et al., 2011; Álvarez et al., 2013). For the SnO_2 bulk exhibit reflection at 2θ 26.7, 34.0 and 51.9° associated to the tetragonal structure of the SnO_2 nanocrystalline (Tong et al., 2010). These SnO_2 broad reflections can be observed in the SnO_2–ZnAl LDH composites which increase with the Sn^{4+} content (Fig. 1). It is known that when Sn^{4+} cations are segregated as SnO_2 oxides over the lamellar structure of the ZnAl LDH, it loses crystallinity as a consequence (Velu et al., 1999; Intissar et al., 2006). XRD patterns of the ZA–Sn4 sample exhibited reflection at 12.9, 33.4 and 36.4°, which were associated to the presence of $Zn_5(CO_3)_2(OH)_6$ compound which have been reported as the precursor phase for the ZnAl LDH formation (Seftel et al., 2007; Zheng et al., 2009; Dimitriev et al., 2011; Koilraj and Srinivasan, 2011; Ahmed et al., 2012a, 2012b; Li et al., 2014; Liu et al., 2014). The formation of ZnAl LDH from $Zn_5(CO_3)_2(OH)_6$ precursor was carried out by the same precipitation method and the XRD analysis (see Fig. S1) showed reflection characteristic of the typical ZnAl LDH, however, it presented additional reflection associated to the $Zn_5(CO_3)_2(OH)_6$ precursor, indicating low transition of $Zn_5(CO_3)_2(OH)_6$ precursor toward ZnAl LDH. Considering that the crystallization of the solid matrix is impeded by the segregation of one of the solid stabilized (Barrera et al., 2004), in our cases for the ZA–Sn4 sample, the transition from the $Zn_5(CO_3)_2(OH)_6$ precursor to ZnAl LDH structure was delayed due to the SnO_2 stabilization, which was segregated in the solid matrix due to the excess of SnO_2. This segregation might cause low Sn^{4+} dispersion in the solid matrix. For the samples with low Sn^{4+} content (0.1, 0.2 and 0.3 mol%) only ZnAl LDH and SnO_2 were detected. However, the presence of this precursor in the rest of the samples cannot be ruled out, due to the presence of the reflection at 12.9°, 2θ.

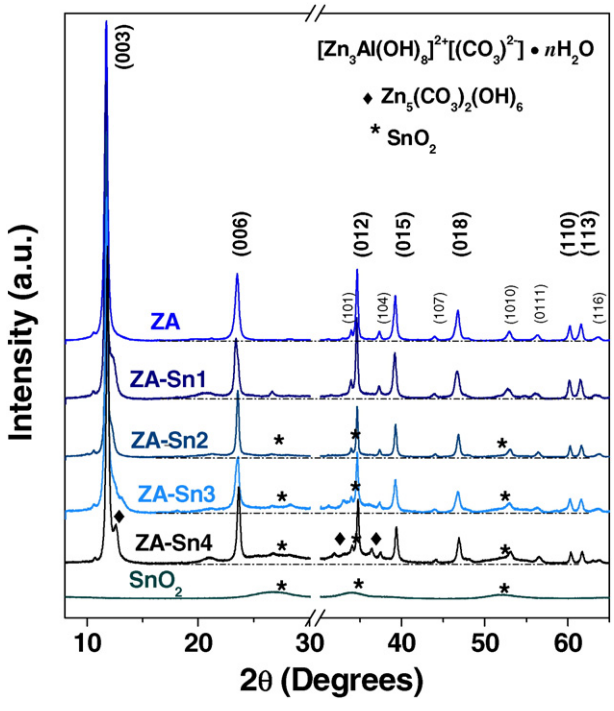

Fig. 1. X-ray diffraction patterns of SnO_2 bulk, ZnAl and SnO_2–ZnAl LDH composites with different Sn^{4+} content.

The values of the lattice parameters of the LDH ("a" and "c", Table 1) were determined from the XRD patterns using the Bragg Law assuming a hexagonal stacking. The parameter value ($a = 3.07 \pm 0.001$ Å) for most of the LDH composites is close to the one reported for ZnAl LDH, whereas the parameter value "c" (22.60 ± 0.1 Å) is reported in the intervals from 22.56 to 26.70 Å (Seftel et al., 2008a, 2008c; Koilraj and Srinivasan, 2011; Zhao et al., 2011; Sahu et al., 2013; Liu et al., 2014). Considering that the parameter $a = 2 \times d_{(110)}$ corresponds to the cation–cation distance within the Brucite layer, and the parameter $c = 3 \times d_{(003)}$ to its thickness, both parameters generally increase when Sn^{4+} cations are inserted into the lattice of the LDH structure due to a partial substitution of Al^{3+} by Sn^{4+}, forming a ternary LDH material (Velu et al., 1999; Tong et al., 2010). However, in our case the modification of the basal spacing parameter of the SnO_2–ZnAl LDH composites is not observed, suggesting that part of the Sn^{4+} cations were preferentially segregated as SnO_2 highly dispersed in the LDH lamellar structure as was mentioned above in XRD section. The parameter "d" (7.53 ± 0.02 Å, Table 1) depends on several factors, including anion size, extent of hydration, and the amount of interlayer anions, among others (Tong et al., 2010). The "d" values suggest that a similar amount of compensating CO_3^{2-} ions and water intercalated in the interlayer region (Ahmed et al., 2012a; Sahu et al., 2013) are retained in the LDH. The analogous size of the thickness of the Brucite layer, where the cavity size (2.75 ± 0.02 Å) is independent on the Sn^{4+} contents, confirming that SnO_2 was preferentially found as well dispersed material in all the LDH structure.

3.2. FTIR spectroscopy studies

The FTIR spectra of the ZnAl LDH (ZA in Fig. 2) exhibit a broad vibration-band centered at 3405 cm^{-1} assigned to the stretching vibrations of adsorbed water and OH groups in the interlamellar LDH structure. The band centered at 1662 cm^{-1} is originated by the bending mode (δ-HOH) of interlayered water molecules (Ahmed et al., 2012a; Sahu et al., 2013). The vibrations bands at 1502 cm^{-1} are attributed to the adsorption of free CO_3^{2-} species or to the antisymmetric O—C—O stretching vibrations and related to the presence of the $Zn_5(CO_3)_2(OH)_6$ compounds. This free CO_3^{2-} species have associated two weak vibration bands at around 1096 cm^{-1} and 835 cm^{-1} from the υ1 symmetric and υ2 out of plane mode, respectively. The strong signal at 1360 cm^{-1} is assigned to symmetric O—C—O stretching vibrations (*v3* mode) of monodentated carbonate (CO_3^{2-}) species of the LDH interlayer structure $[Zn_3Al(OH)_8]^{2+}[(CO_3)^{2-}]\cdot nH_2O$ (Seftel et al., 2007; Sahu et al., 2013; Liu et al., 2014). For all the SnO_2–ZnAl LDH composites, the

Table 1
Lattice parameter and band-gap energy of ZnAl LDH, SnO_2–ZnAl LDH composites with different Sn^{4+} content and SnO_2–ZnAl^{Imp} impregnated.

Sample	Lattice parameter (Å)*				Band-gap (eV)
	$d_{(003)}$	$c = 3 \times d_{(003)}$	$a = 2 \times d_{(110)}$	Cavity	
ZA	7.53	22.60	3.07	2.73	5.2
ZA–Sn1	7.57	22.70	3.07	2.77	4.3
ZA–Sn2	7.53	22.60	3.07	2.73	4.2
ZA–Sn3	7.52	22.56	3.07	2.72	4.2
ZA–Sn4	7.55	22.65	3.07	2.75	3.8, 3.3[a]
ZA–Sn3^{Imp}	7.50	22.51	3.07	2.70	3.9, 3.3[a]

* Determined by using Bragg law.
[a] Band-gap energy of the ZnO.

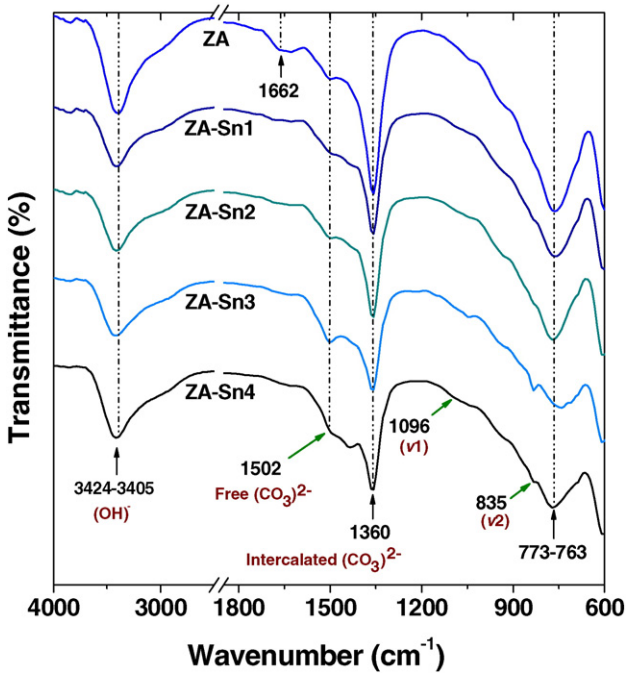

Fig. 2. FTIR spectrum of ZnAl and SnO_2–ZnAl LDH composites with different Sn^{4+} content.

vibration band of the —OH group at 3405 cm^{-1} was slightly shifted to 3424 cm^{-1} as the Sn^{4+} content was increased, suggesting an increasing in the interactions of the —OH vibration bonds with the LDH interlayer structure. The vibration band (1502 cm^{-1}) related to the free CO_3^{2-} species increases in intensity, whereas the vibration band (1360 cm^{-1}) that correspond to intercalated CO_3^{2-} species on the interlayer LDH structure decreases when the Sn^{4+} content increases. The relative concentration of each CO_3^{2-} species (Table 2), determined by the integrating area under the curve of each intensity, confirms this behavior. In addition, it is observed that the relative concentration of interlayered water molecules (δ-HOH) is also decreased. Summarizing, low amounts of zinc carbonate precursor is formed in the composite at low Sn^{4+} content, it was evidenced in the LDH composite with 0.4 mol% of Sn^{4+}. Finally, for all samples, the vibration band at 773 cm^{-1} is characteristic of the translation mode of Al–OH (Seftel et al., 2007; Liu et al., 2014).

3.3. Morphology, structural and composition analyses

SEM, TEM and HRTEM images of the selected ZA samples are shown in Fig. 3a, b and c, respectively. For the ZnAl LDH, the SEM and TEM image exhibits the formation of laminar structures with sheets-like morphology with different orientations and heterogeneous sizes from 50 to 200 nm, including superimposed conglomerates. The TEM image also indicates the thin nature of the ZnAl-LDH sheets. This kind of morphology has been reported for ZnAl LDH with a Zn/Al ratio of 3 (Ahmed et al., 2012b; Liu et al., 2014). The FFT pattern from the HRTEM image of the highlighted nanoparticle in the marked region by a white line (Fig. 3c), exhibits lattice fringes that can be indexed to hexagonal structures, indicating that material corresponds to highly crystalline LDH (Zhao et al., 2010). For the ZA–Sn3 composite, when the SnO_2 is one step formed together with ZnAl LDH, the morphology of the flakes or sheets-like is distorted or fully destroyed to an amorphous or conglomerated particles (Fig. 3d and e). The TEM image shows a micrograph with clearness and darkness zones more or less homogeneous, indicating homogeneous small particle size (about of 50 nm) but some particles have larger thickness. The corresponding FFT pattern in the marked region by a white line and white circle (Fig. 3f), exhibit two lattice fringes that can be indexed to hexagonal structures of the LDH and the rutile crystal structures of SnO_2 highly crystalline (Peche-Herrero et al., 2014). Thus the HRTEM image clearly reveals the on step formation of heterostructures SnO_2–ZnAl within the LDH interface (composites-type), which would have facilitated to carry out electron transfer process in the interface and would increases the photocatalytic activity (Peche-Herrero et al., 2014). In the case for ZA–Sn4, despite that the heterostructure SnO_2–ZnAl is formed (Fig. 3h), the TEM image (Fig. 3g) exhibits both sheet and rod-like morphology, where the rod-particle is characteristic of the SnO_2 formation, suggesting that part of SnO_2 was segregated.

In order to confirm the distribution of SnO_2 within the ZnAl LDH material, elemental analysis using EDX elemental mapping was conducted for the ZA–Sn3 and ZA–Sn4 sample. These materials include the elements O, Zn and Al (not shown) but the EDX elemental mappings of ZA–Sn3 from a selected area (Fig. 3i) shows that the SnO_2 is dispersed and uniformly distributed in all the materials, whereas for the ZA–Sn4 sample, confirms that the SnO_2 is poorly dispersed (Fig. 3j), indicating that it was segregated.

According to the analysis by atomic absorption spectroscopy (AAS), the molar ratio Zn/(Al + Sn) (Table 3) is lesser than that obtained for the ZnAl LDH, suggesting that the molar ratio was affected by Sn^{4+} content. The mol% of Sn^{4+} for the LDH composites at low Sn^{4+} contents (0.1–0.3) was almost closer to the theoretical value. However, for the ZA–Sn4 sample, the mol% of Sn^{4+} (Table 3) was lower to the theoretical value, despite that the reflection peaks of SnO_2 was increased (Fig. 1), it was due to the inhomogeneous distribution. So, the optimal value of Sn^{4+} for the incorporation into ZnAl LDH material could be 0.3 mol%.

Table 2
Relative concentration of the —OH and CO_3^{2-} species for all the samples.

Sample	Relative concentration (%)[a]			
	—OH	δ-HOH	Free $(CO_3)^{2-}$	Intercalated $(CO_3)^{2-}$
ZA	63.66	4.99	6.48	24.85
ZA–Sn1	60.45	3.68	0.00	35.86
ZA–Sn2	61.89	3.33	7.64	27.12
ZA–Sn3	62.15	2.40	11.31	24.13
ZA–Sn4	65.36	1.73	16.96	15.94

[a] Determined by integration of the area under the curve of the intensity.

3.4. Surface analysis by XPS

The surface chemical composition of the ZA, ZA–Sn3 and ZA–Sn4 sample was determined by XPS. The survey spectrum (Fig. 4) for ZnAl LDH showed emissions of Al, Zn and O elements. The binding energy for Al2p at 74.2 eV is associated to an aluminum hydroxide species $Al(OH)_n$ (Solis-Maldonado et al., 2014). The binding energy of Zn3d, Zn3p, Zn3s, $Zn2p_{3/2}$ and $Zn2p_{1/2}$ and the asymmetric Auger lines ($ZnL_3M_{45}M_{45}$), confirm the presence of Zn element in the LDH. The Auger signals positioned at higher energy peak (499.2 eV) is ascribed to the bonding of Zn–OH (Arkhipushkin et al., 2014). The high resolution XPS spectrum of oxygen show asymmetric shoulder peak which indicate that there are several chemical states depending on the binding energies. Thus, O1s spectrum peak is deconvoluted into four peaks centered at 530.9, 531.7, 532.2 and 533.2 eV. The first peak is attributed to bonding metal–oxygen (M—O—M) like ZnO, while the peak at 531.7 eV is ascribed to metal–hydroxyl groups or water molecule coordinated to metal cations (M—OH, M—O—CR) (Cottineau et al., 2014; He et al., 2015b). The peak at 532.2 is related to oxygen from OC—R bonds and the last peak is due to the adsorbed hydroxyl groups (Celebioglu et al., 2014).

The survey spectrum (Fig. 4) for SnO_2–ZA LDH composites showed additional emissions of Sn elements, where the high resolution XPS spectrum of Sn3d exhibited two symmetric peaks at 486.7 eV and at 495.2 eV, corresponding to $Sn3d_{5/2}$ and to $Sn3d_{3/2}$, respectively, although this last peak is overlapped with the Auger signal of Zn^{2+}

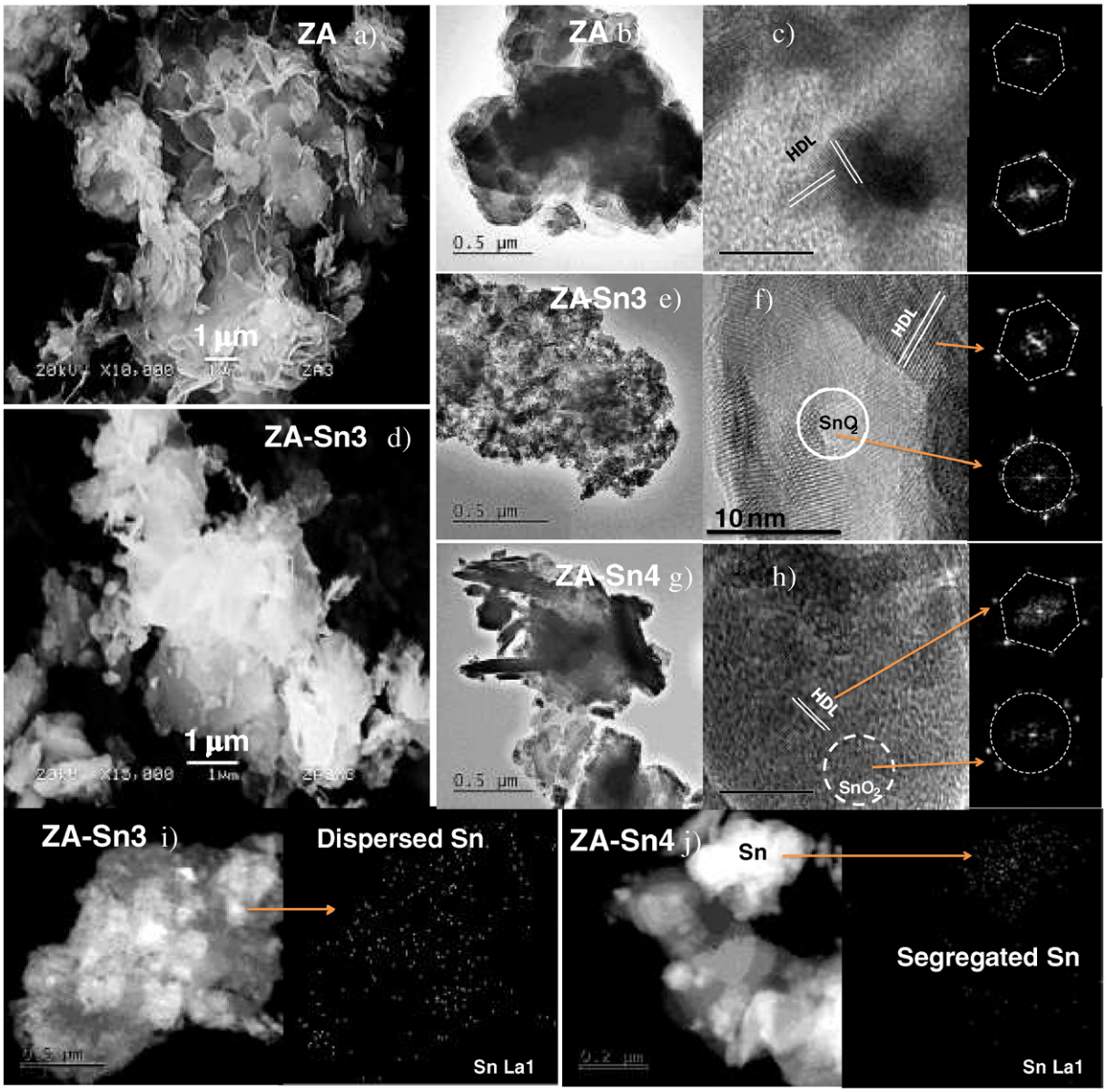

Fig. 3. SEM (a, d), TEM (b, e) and HRTEM (c, f) of ZA LDH and ZA–Sn3 composite, respectively and TEM (g) and HRTEM (h) of ZA–Sn4 composite. EDX elemental mapping for ZA–Sn3 (i) and ZA–Sn4 (j).

(LMM). The spin–orbit splitting of 8.5 eV indicates the presence of Sn^{4+} cations, which is in agreement to that reported for SnO_2 (Jia et al., 2014). The high resolution XPS spectrum of oxygen for the composite was different. For the ZA–Sn3 composite, the oxygen spectrum peak is deconvoluted into two peaks associated to bonding metal–oxygen and metal–OH groups, but for ZA–Sn4, the oxygen spectrum peak is additionally deconvoluted into the OC—R bonds and to the adsorbed OH groups present in the LDH.

Table 3
Data of atomic composition, molar ratio of Zn/(Al + Sn) and (Al + Sn) for the ZnAl LDH and SnO_2–ZnAl LDH composites with different Sn^{4+} content.

Sample	Atomic composition* (wt.%)			Zn/(Al + Sn) molar ratio[a]	(Al + Sn) mol%[a]	
	Zn^{2+}	Al^{3+}	Sn^{4+}		Al^{3+}	Sn^{4+}
ZA	43.48	7.37	0.00	2.43	1.00	0.00
ZA–Sn1	40.10	6.57	2.93	2.29	0.91	0.09
ZA–Sn2	35.23	6.80	5.21	1.82	0.85	0.15
ZA–Sn3	35.14	4.54	7.04	2.36	0.74	0.26
ZA–Sn4	34.37	4.98	6.62	2.19	0.77	0.23

* Determined by atomic absorption spectroscopic.
[a] Experimental calculations.

3.5. UV–Vis diffuse reflectance spectroscopy

The UV–Vis diffuse reflectance spectrum for the ZnAl LDH shows an absorption band at 210–240 nm (Fig. 5) related to the band gap energy of 5.2 eV. According to the literature, this absorption edge is due to the electronic transition of ZnAl LDH from the O2p state to the metal *ns* or *np* levels ($n = 4$ for Zn and $n = 3$ for Al) (Seftel et al., 2008a, 2008b; Ahmed et al., 2011). For the SnO_2 bulk dried at 100 °C, it exhibits an absorption band at 262 nm corresponding to hexacoordinated Sn^{4+} ions (Seftel et al., 2008c) associated to the band gap energy of 3.7 eV (see Fig. S2). For the SnO_2–ZnAl LDH composites, additional to the absorption band at 215 nm which corresponds to the electronic transition of ZnAl LDH, these spectra exhibit a new absorption band appeared at 254 nm, which increases as the Sn^{4+} was loaded at the ZnAl LDH. This increasing absorption is related to the presence of SnO_2 crystallites,

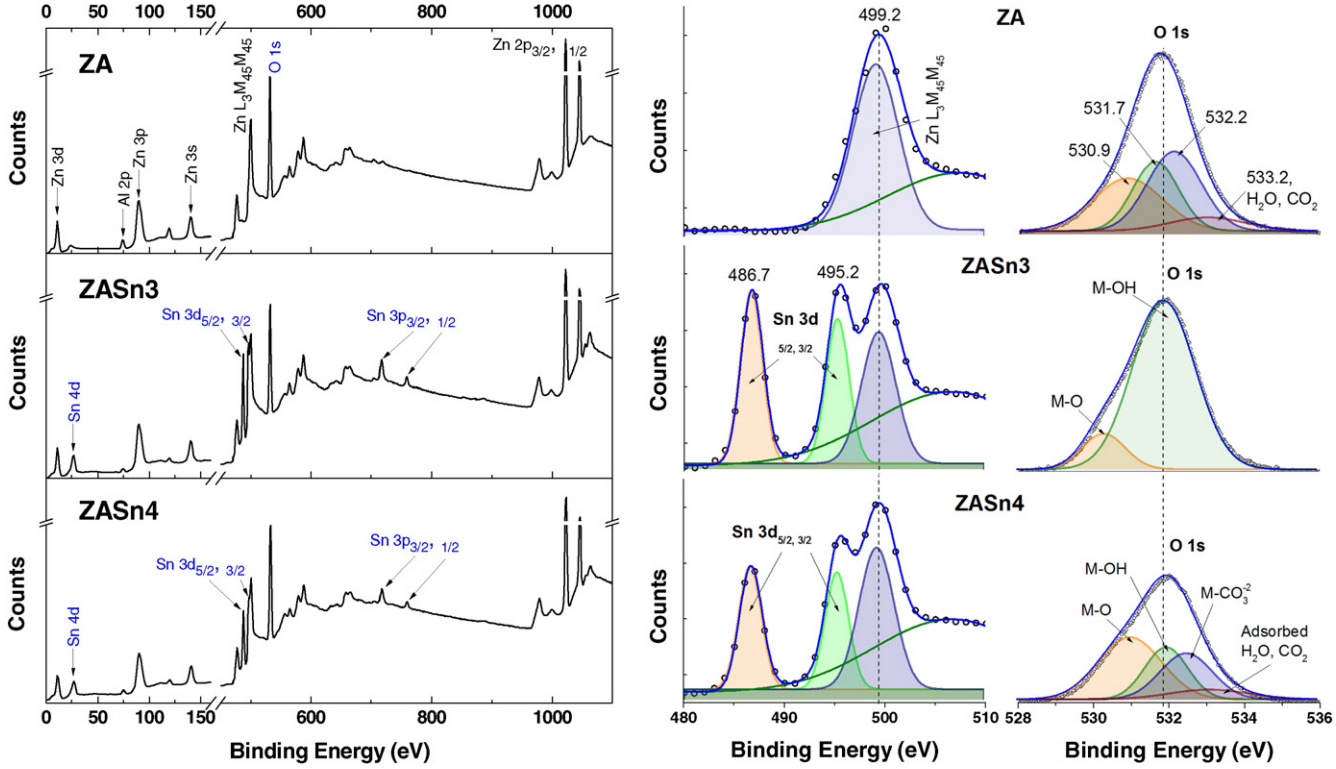

Fig. 4. XPS spectra for the ZA LDH, ZA–Sn3 and ZA–Sn4 composites with respective high resolution spectra of Sn3d and O1s.

however, for the LDH composites at low Sn^{4+} contents, the observed blue-shift absorption, associated to the band gap energy between 4.2 and 4.3 eV (Table 1), may be attributed to the effect of the small crystal size of SnO_2 (Yao et al., 2014).

In opposite, for the ZA–Sn4 composite (high Sn^{4+} content), one additional broad band (310–360 nm) centered mainly at 354 nm was detected, which was associated to band gap energy of 3.3 eV. Considering that when ZA–Sn4 sample was dried at 200 °C, ZnO nanocrystalline was detected by XRD, being more evident when it was annealed at 450 °C (Fig. S3a) and its optical absorption exhibited the band at 354 nm, which was increased in the sample containing more crystalline ZnO (sample at 450 °C, Fig. S3b). The presence of the ZnO in the ZnAl LDH at Zn/Al of 3–4 molar ratio, has been observed with a simple drying at 85 and 120 °C (Patzkó et al., 2005), and it has been assigned to the band gap energy of 3.5 eV (Ahmed et al., 2012b). Therefore the absorption band at 354 nm in the ZA–Sn4 composite dried at 100 °C may be due to the presence of the crystalline ZnO (Seftel et al., 2008a) despite that it was not possible to be detected by XRD due to the limit of detection. The small traces of $Zn_5(CO_3)_2(OH)_6$ precursor does not affect the optical-electronic property in ZA–Sn4 composite because of the electronic transition of the precursor appearing at 196 nm (see Fig. S4), which is similar to that of ZnAl-LDH.

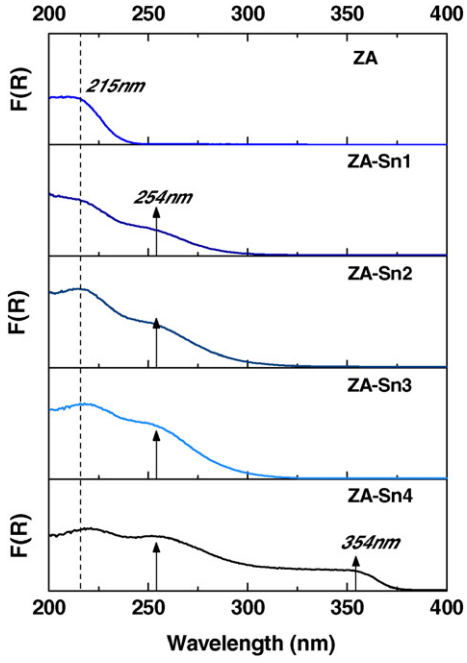

Fig. 5. UV–Vis diffuse reflectance spectrum of ZnAl and SnO_2–ZnAl LDH composites with different Sn^{4+} content.

3.6. Characterization of SnO_2–$ZnAl^{Imp}$ LDH

The XRD patterns of the SnO_2–$ZnAl^{Imp}$ LDH composite obtained by the SnO_2 impregnation, Fig. 6a, showed reflection of the main planes characteristics of the typical ZnAl LDH structures with intercalated carbonate ions. In addition, the impregnated sample exhibited reflection corresponding to the formed $Zn_5(CO_3)_2(OH)_6$ compounds. SnO_2 was not observed, it could be due to the SnO_2 is well dispersed on the lamellar surface or because the crystallite size is smaller than the limit of detection (Bowering et al., 2007). The values of the lattice parameters ("a", "c" and "d", Table 1) are close to the one reported for ZnAl LDH.

The UV–Vis diffuse reflectance spectrum (Fig. 6b) shows an absorption band at 218 and 254 nm associated to the band gap energy of 4.0 eV, which are assigned to the presence of crystalline SnO_2. Additionally, it exhibits an absorption band at 354 nm, which was previously related to the presence of ZnO (see Fig. S3b). The FTIR spectra (Fig. 6c) showed the vibration bands at 3448, 1502, 1360 and 763 cm^{-1} assigned to stretching vibrations of adsorbed water in the interlamellar LDH structure, of free CO_3^{2-} species, of monodentated CO_3^{2-} species of the interlayer of the LDH structure and of the translation mode of Al–OH.

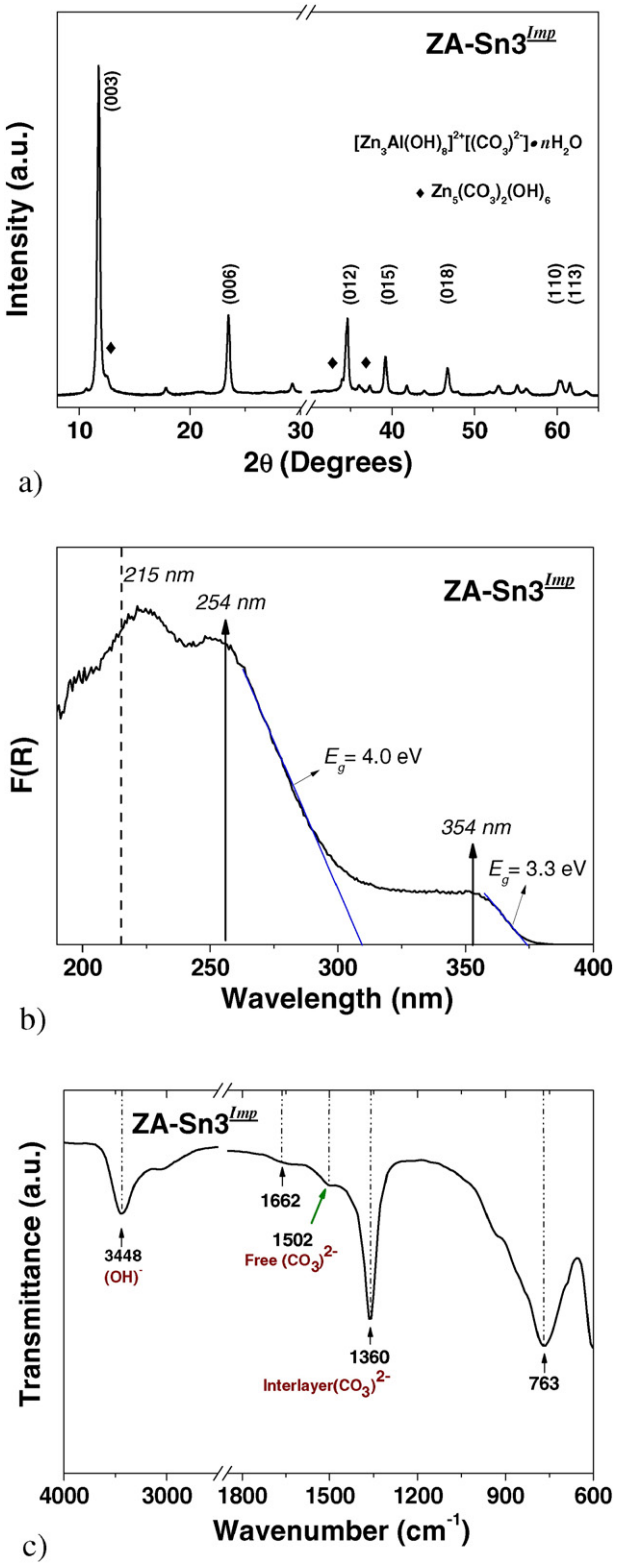

Fig. 6. a) X-ray diffraction patterns, b) UV–Vis diffuse reflectance spectra and c) FTIR spectra of ZnAl LDH impregnated with 0.3 mol% of Sn^{4+}.

3.7. Photocatalytic activities

The UV–Vis absorbance spectra of the phenol adsorption and photodegradation as time progressed (Fig. S5a) for the selected ZA–Sn3 photocatalysts, show that during the adsorption step in dark condition, the phenol was not adsorbed (dashed line), however during the UV-irradiation step, the absorption bands at 220 and 269 nm, corresponding to aromatic ring and phenol group, respectively, were drastically reduced in 120 min. An additional small absorption band at 280 nm was observed during the photodegradation reaction indicating the formation of intermediates (Su et al., 2012) which were totally mineralized after 120 min of irradiation. The rest of the samples showed the same tendency, so, during the UV irradiation step, the bands corresponding to phenol were reduced in along irradiation time. Previous studies showed that the photodegradation of phenol by using SnO_2 bulk was negligible (Mendoza-Damián et al., 2015).

The profile of the kinetic reaction (Fig. S5b) can be adjusted to a pseudo first order reaction ($\ln(C_0 / C) = kt$). The experimental data of the each sample including the TiO_2 as a reference were fitted to the equation above and the value of the rate constant, k, was summarized in Table 4. The calculated rate constant for TiO_2–P25 was 4.2×10^{-3} min^{-1}, 2.4×10^{-3} min^{-1} for ZA and 9.8×10^{-3} min^{-1} for ZA–Sn3 photocatalysts in the phenol photodegradation, showing that the ZA–Sn3 solid is the most active photocatalyst. The low photoactivity of ZnAl LDH in the phenol photodegradation can be due to low absorptivity in the UV region, however, it has been related to the presence of the $Zn(OH)_2$ and ZnO (Patzkó et al., 2005). For the ZA–Sn3 sample its photoactivity is four times more active than unmodified ZnAl LDH and twice more active than the one obtained for the reference photocatalysts TiO_2–P25 (Fig. 7a). This result suggests that when the SnO_2 is one step formed together with ZnAl LDH, the formed heterostructure has a positive effect on the photocatalytic properties, may be due to the UV absorption capacity and to the enhanced efficiency of the electron–hole charge separation. This finding showed correlation with UV–Vis diffuse reflectance spectroscopy results and the spectrum emission of the UV lamp at 254 nm. In opposite for the ZA–Sn4 photocatalyst, despite of its UV absorption capacity, the presence of small traces of nanocrystalline ZnO and the SnO_2 segregated produces a negative effect on its photocatalytic activity.

The ZA-Sn3^{Imp} photocatalyst showed low activity (3.5×10^{-3} min^{-1}) in the phenol photodegradation. Despite of that, the UV absorption capacity was extended by the SnO_2 impregnation, the low activity was probably due to the SnO_2 dispersed only on the LDH surface, where the LDH act as support without the heterostructure formation. In this case, the UV-activated SnO_2 is capable to photogenerate the e^-/h^+ pairs, however, the separation of these charges was not achieved. Therefore, the SnO_2 formed together with ZnAl LDH structure in one step forming a heterostructure resulted better than the impregnated SnO_2, producing a synergistic effect between the SnO_2 and ZnAl LDH and facilitating the electron transfer process at the interface.

The TOC analysis of the irradiated solution was performed in order to get complementary information of the degree of mineralization achieved by the photocatalysts (Fig. 7b). It can be seen that a correlation between the photodegradation of phenol and its total mineralization was reached, and the ZA–Sn3 photocatalyst achieved up to 91% of phenol mineralization within 120 min of reaction.

Table 4
Kinetic parameters (k and $t_{1/2}$) and TOC analyses for the photocatalysts evaluated in the photodegradation of phenol.

Sample	k ($\times 10^{-3}$) (min^{-1})[a]	$t_{1/2}$ (min)	Mineralization (%)[b]
ZA	2.36	293.71	21.15
ZA–Sn1	5.41	128.12	63.66
ZA–Sn2	6.51	106.47	82.03
ZA–Sn3	9.75	71.09	90.98
ZA–Sn4	7.01	98.88	60.61
TiO_2–P25	4.23	163.86	29.24
ZA–Sn3^{Imp}	3.48	199.18	13.58

[a] Determined by using spectroscopy UV–Vis data.
[b] Determined by using TOC data.

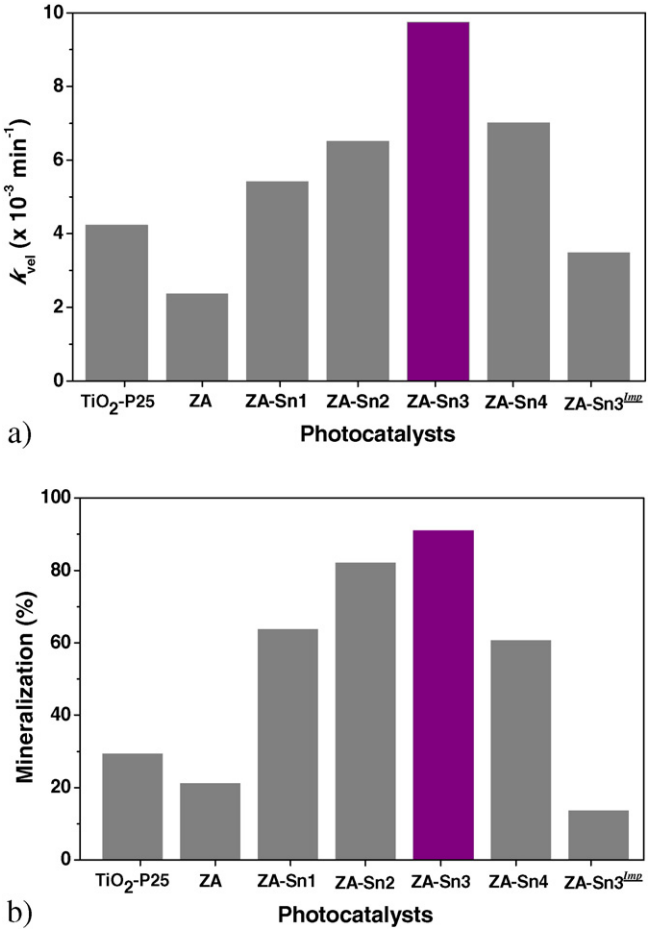

Fig. 7. a) Apparent pseudo first order rate constant for the photodegradation of phenol and b) percent of mineralization determined by TOC analysis of ZnAl, SnO_2–ZnAl LDH photocatalysts and ZnAl LDH impregnated with SnO_2, including TiO_2–P25 as reference catalyst.

3.8. Formation of •OH radical

To explore the mechanism of phenol photodegradation, the formation of active hydroxyl radicals (•OH) upon irradiation was monitored, which is typically considered as the most important oxidative intermediate in photocatalytic reactions. This formed •OH radical was trapped by terephthalic acid, producing fluorescent of the 2-hydroxyterephthalic acid, which is detected by its emission at around 425 nm (Milan-Segovia et al., 2007). As shown in Fig. 8a, the fluorescence signals associated to the formation of 2-hydroxy terephthalic acid generated by using the ZA–Sn3 LDH photocatalyst in absence of phenol, greatly increases as the time progress during the first 10 min. The linear relationship between fluorescence intensity and irradiation time (Fig. 8b) can be related to the rate of •OH radical generation, where the generation rate (448 M min^{-1}) for the ZnAl LDH solid is so low like that of the photolysis (331 M min^{-1}) but when LDH contains 0.3 mol% of Sn^{4+} dispersed in all the LDH structure, the rate of radical generation (1854 M min^{-1}) increases up to 4.1 times more than the ZnAl LDH unmodified sample. Considering that the optical density of ZA–Sn3 composite at 254 nm is 6.8, by using 200 mg of mass the UV absorption is 27 times more than for the phenol (0.25) and as a consequence that amount of •OH radical that could be generated by the phenol is negligible. This result suggests that the oxidation processes of the phenol molecule follow the known mechanism via the •2OH radical generation.

3.9. Mechanism of reaction

When the ZnAl LDH dried at 100 °C (intercalated with carbonate ions) was irradiated by UV light, •OH radicals were poorly photogenerated since of ZnAl LDH cannot be fully activated (Fig. 9a), giving a low photocatalytic activity like the one obtained by photolysis. In opposite, when small crystallites of SnO_2 are formed together with the ZnAl LDH structure in one step, the UV absorption capacity of the ZnAl LDH is extended, achieving a synergistic effect between them and as a consequence the more e^-/h^+ pair charge can be photogenerated and separated. Increasing the Sn^{4+} contents up to 0.3 mol%, the e^-/h^+ pair generation was achieved (Fig. 9b), allowing the formation of more •OH radicals reacting with the organic phenolic compound. In opposite, when 0.3 mol% of Sn^{4+} was impregnated on the ZnAl LDH surface (ZA–Sn3^{Imp}), the synergistic effect was not achieved.

4. Conclusions

Composites of SnO_2–ZnAl LDH were successfully synthesized by co-precipitation in one step, obtaining an optimal value of the Sn^{4+} content of 0.3 mol%. The SnO_2 formed together with ZnAl LDH structure forms a

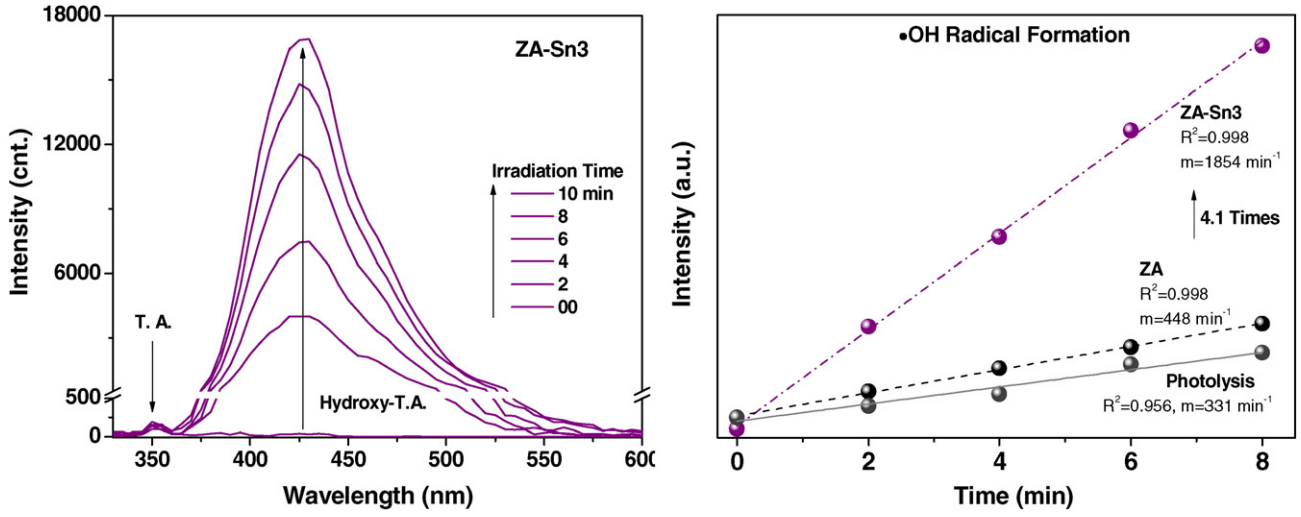

Fig. 8. a) Fluorescence spectrum of hydroxyl terephthalic acid during the irradiation of ZA–Sn3 composite and b) profile of the lineal rate of •OH radical formation for the selected photocatalyst in the absence of phenol.

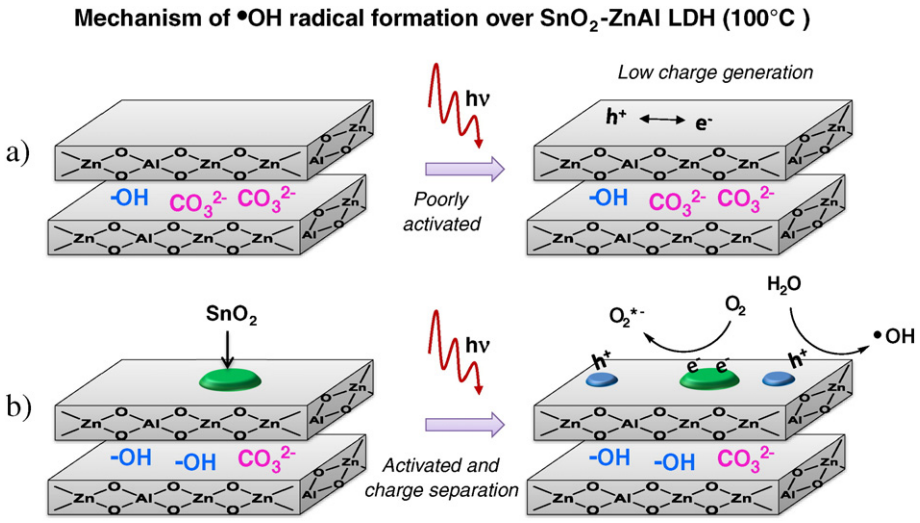

Fig. 9. Schematic representation of the mechanism of •OH radical formation over SnO_2–ZnAl LDH composite.

heterostructured material, where the small crystallite of SnO_2 is dispersed in all the LDH matrix. High SnO_2 contents (0.4 mol%) cannot be fully dispersed on the LDH structure and as a consequence the segregated SnO_2 delayed the crystallization of the $Zn_5(CO_3)_2(OH)_6$ precursor towards the ZnAl LDH final. The dried SnO_2–ZnAl LDH composite with 0.3 mol% of Sn^{4+}, exhibited the highest photocatalytic activity compared to the ZnAl LDH impregnated with SnO_2, and it was even more active than the TiO_2–P25 as reference. Its high photoactivity was related to the absorption capacity in the UV region and to the synergistic effect of the heterostructured formed between SnO_2 and ZnAl LDH, improving the (e^-/h^+) pair generation and separation.

Acknowledgments

The authors would like to acknowledge the financial support provided by CONACyT (Project 154994). Guadalupe Mendoza Damián would like to thank CONACyT for a scholarship granted (scholarship number: 252087). The authors would like to acknowledge to Ing. Elías Acosta León for the atomic absorption analysis and PhD. Alma Mireya Arrieta Castañeda from UAM-Iztapalapa for the HRTEM and EDX analysis.

Appendix A. Supplementary data

Supplementary data to this article can be found online at http://dx.doi.org/10.1016/j.clay.2015.12.007.

References

Ahmed, N., Shibata, Y., Taniguchi, T., Izumi, Y., 2011. Photocatalytic conversion of carbon dioxide into methanol using zinc–copper–M(III) (M = aluminum, gallium) layered double hydroxides. J. Catal. 279, 123–135.
Ahmed, A.A.A., Talib, Z.A., Hussein, M.Z., 2012a. Thermal, optical and dielectric properties of Zn–Al layered double hydroxide. Appl. Clay Sci. 56, 68–76.
Ahmed, A.A.A., Talib, Z.A., Hussein, M.Z., Zakaria, A., 2012b. Zn–Al layered double hydroxide prepared at different molar ratios: preparation, characterization, optical and dielectric properties. J. Solid State Chem. 191, 271–278.
Álvarez, M.G., Chimentão, R.J., Barrabés, N., Föttinger, K., Gispert-Guirado, F., Kleymenov, E., Tichit, D., Medina, F., 2013. Structure evolution of layered double hydroxides activated by ultrasound induced reconstruction. Appl. Clay Sci. 83–84, 1–11.
Arkhipushkin, I.A., Pronin, Y.E., Vesely, S.S., Kazansky, L.P., 2014. Electrochemical and XPS study of 2-mercaptobenzothiazole nanolayers on zinc and copper surface. Int. J. Corros. Scale Inhib. 3 (2), 78–88.
Barrera, M.C., Viniegra, M., Escobar, J., Vrinat, M., de los Reyes, J.A., Murrieta, F., García, J., 2004. Highly active MoS_2 on wide-pore ZrO_2–TiO_2 mixed oxides. Catal. Today 98, 131–139.
Bowering, N., Croston, D., Harrison, P.G., Walker, G.S., 2007. Silver modified Degussa P25 for the photocatalytic removal of nitric oxide. Int. J. Photogr. 2007, 1–8.
Bravo-Suárez, J.J., Páez-Mozo, E.A., Oyama, S.T., 2004. Microtextural properties of layered double hydroxides: a theoretical and structural model. Microporous Mesoporous Mater. 67, 1–17.
Cavani, F., Trifirò, F., Vaccari, A., 1991. Hydrotalcite-type anionic clays: preparation, properties and applications. Catal. Today 11, 173–301.
Celebioglu, A., Vempati, S., Ozgit-Akgun, C., Biyikliab, N., Uyar, T., 2014. Water-soluble non-polymeric electrospun cyclodextrin nanofiber template for the synthesis of metal oxide tubes by atomic layer deposition. RSC Adv. 4, 61698–61705.
Cottineau, T., Rouet, A., Fernandez, V., Brohana, L., Richard-Plouet, M., 2014. Intermediate band in the gap of photosensitive hybrid gel based on titanium oxide: role of coordinated ligands during photoreduction. J. Mater. Chem. A 2, 11499–11508.
Das, N., Samal, A., 2004. Synthesis, characterisation and rehydration behavior of titanium (IV) containing hydrotalcite like compounds. Microporous Mesoporous Mater. 72, 219–225.
Dimitriev, Y., Gancheva, M., Iordanova, R., 2011. Synthesis of ZnO by mechanochemical decomposition of zinc carbonate hydroxide. J. Univ. Chem. Technol. Metallurgy. 46, 243–248.
Guo, Z., Ma, R., Li, G., 2006. Degradation of phenol by nanomaterial TiO_2 in wastewater. Chem. Eng. J. 119, 55–59.
He, W., Wang, R., Zhang, L., Zhu, J., Xiang, X., Lia, F., 2015a. Enhanced photoelectrochemical water oxidation on a $BiVO_4$ photoanode modified with multifunctional layered double hydroxide nanowalls. J. Mater. Chem. A 3, 17977–17982.
He, W., Yang, Y., Wang, L., Yang, J., Xiang, X., Yan, D., Li, F., 2015b. Photoelectrochemical water oxidation efficiency of a core/shell array photoanode enhanced by a dual suppression strategy. ChemSusChem 8, 1568–1576.
Herrmann, J.-M., 2010a. Photocatalysis fundamentals revisited to avoid several misconceptions. Appl. Catal. B Environ. 99, 461–468.
Herrmann, J.-M., 2010b. Fundamentals and misconceptions in photocatalysis. J. Photochem. Photobiol. A Chem. 216, 85–93.
Intissar, M., Malherbe, F., Prévot, V., Leroux, F., 2006. Evidences of segregated SnO_2 type nanoparticles coating layered double hydroxide at moderate temperature. J. Colloid Interf. Sc. 299, 747–753.
Jia, T., Chen, J., Deng, Z., Fu, F., Zhao, J., Wang, X., Long, F., 2014. Facile synthesis of Zn-doped SnO2 dendrite-built hierarchical cube-like architectures and their application in lithium storage. Mater. Sc. Engin. B 189, 32–37.
Koilraj, P., Srinivasan, K., 2011. High sorptive removal of borate from aqueous solution using calcined ZnAl layered double hydroxides. Ind. Eng. Chem. Res. 50, 6943–6951.
Li, Z., Yang, B., Zhang, S., Wang, B., Xue, B., 2014. A novel approach to hierarchical sphere-like ZnAl-layered double hydroxides and their enhanced adsorption capability. J. Mater. Chem. A. 2, 10202–10210.
Liu, J., Song, J., Xiao, H., Zhang, L., Qin, Y., Liu, D., Hou, W., Du, N., 2014. Synthesis and thermal properties of ZnAl layered double hydroxide by urea hydrolysis. Powder Technol. 253, 41–45.
Mendoza-Damián, G., Tzompantzi, F., Mantilla, A., Lartundo-Rojas, L., 2013. Photocatalytic degradation of 2,4-dichlorophenol with MgAlTi mixed mixedoxides catalysts obtained from layered double hydroxides. J. Hazard. Mater. 263P, 67–72.
Mendoza-Damián, G., Hernández-Gordillo, A., Tzompantzi, F., Gómez, R., 2015. Photocatalytic degradation of phenol using Al_2O_3–SnO_2 mixed oxide. J. Nanosci. Nanotechnol. 15, 7258–7261.
Milan-Segovia, N., Wang, Y., Cannon, F.S., Voigt, R.C., James, C., Furness, J., 2007. Comparison of hydroxyl radical generation for various advanced oxidation combinations as applied to foundries. Ozone Sci. Eng. 29, 461–471.

Mohapatra, L., Parida, K., 2012. Zn–Cr layered double hydroxide: visible light responsive photocatalyst for photocatalytic degradation of organic pollutants. Sep. Purif. Technol. 91, 73–80.

Parida, K.M., Mohapatra, L., 2012. Carbonate intercalated Zn/Fe layered double hydroxide: a novel photocatalyst for the enhanced photo degradation of azo dyes. Chem. Eng. J. 179, 131–139.

Parida, K.M., Dash, S.S., Das, D.P., 2010. Physico-chemical characterization and photocatalytic activity of zinc oxide prepared by various methods. J. Colloid Interface Sci. 298-2, 787–793.

Patzkó, A., Kun, R., Hornok, V., Dékány, I., Engelhardt, T., Schall, N., 2005. ZnAl-layer double hydroxides as photocatalysts for oxidation of phenol in aqueous solution. Colloids Surf. A Physicochem. Eng. Asp. 265, 64–72.

Peche-Herrero, M.A., Maestre, D., Ramírez-Castellanos, J., Cremades, A., Piqueras, J., González-Calbet, J.M., 2014. The controlled transition-metal doping of SnO_2 nanoparticles with tunable luminescence. CrystEngComm 16, 2969–2976.

Sahu, R.K., Mohanta, B.S., Das, N.N., 2013. Synthesis, characterization and photocatalytic activity of mixed oxides derived from ZnAlTi ternary layered double hydroxides. J. Phys. Chem. Solids 74, 1263–1270.

Seftel, E.M., Popovici, E., Podeb, V., Bandur, G., 2007. Synthesis, characterization and thermal behavior of hydrotalcite-type Mg_xZn_yAl. Rev. Roum. Chim. 52 (11), 1033–1037.

Seftel, E.M., Popovici, E., Mertens, M., Witte, K.D., Tendeloo, G.V., Cool, P., Vansant, E.F., 2008a. Zn–Al layered double hydroxides: synthesis, characterization and photocatalytic application. Microporous Mesoporous Mater. 113, 296–304.

Seftel, E.M., Popovici, E., Mertens, M., Stefaniak, E.A., Grieken, R.V., Cool, P., Vansant, E.F., 2008b. Sn^{IV}-containing layered double hydroxides as precursors for nano-sized ZnO/SnO2 photocatalysts. Appl. Catal. B Environ. 84, 699–705.

Seftel, E.M., Popovici, E., Mertens, M., Cool, P., Vansant, E.F., 2008c. Infrared and Raman spectroscopic study of Sn-containing Zn/Al-layered double hydroxides. J. Optoelectron. Adv. Mater. 10, 3477–3481.

Sobczynski, A., Duczmal, L., Zmudzinski, W., 2004. Phenol destruction by photocatalysis on TiO_2: an attempt to solve the reaction mechanism. J. Mol. Catal. A Chem. 213, 225–230.

Solis-Maldonado, C., Rivera De la Rosa, J., Lucio-Ortiz, C., Hernández-Ramírez, A., Castillón-Barraza, F., Valente, J.S., 2014. Low concentration Fe-doped alumina catalysts using sol–gel and impregnation methods: the synthesis, characterization and catalytic performance during the combustion of trichloroethylene. Materials 7, 2062–2086.

Su, R., Tiruvalam, R., He, Q., Dimitratos, N., Kesavan, L., Hammond, C., Lopez-Sanchez, J.A., Bechstein, R., Kiely, C.J., Hutchings, G.J., Besenbacher, F., 2012. Promotion of phenol photodecomposition over TiO_2 using Au, Pd, and Au-Pd nanoparticles. ACS Nano 6, 6284–6292.

Tong, D.S., Zhou, C.H., Li, M.Y., Yu, W.H., Beltramini, J., Lin, C.X., Xu, Z.P., 2010. Structure and catalytic properties of Sn-containing layered double hydroxides synthesized in the presence of dodecylsulfate and dodecylamine. Appl. Clay Sc. 48, 569–574.

Tzompantzi, F., Mantilla, A., Bañuelos, F., Fernández, J.L., Gómez, R., 2011. Improved Photocatalytic degradation of phenolic compounds with ZnAl mixed oxides obtained from LDH materials. Top. Catal. 54, 257–263.

Velu, S., Suzuki, K., Osaka, T., Ohashi, F., Tomura, S., 1999. Synthesis of new Sn incorporated layered double hydroxides and their evolution to mixed oxides. Mater. Res. Bull. 34, 1707–1717.

Xiang, X., Xie, L., Li, Z., Li, F., 2013. Ternary $MgO/ZnO/In_2O_3$ heterostructured photocatalysts derived from a layered precursor and visible-light-induced photocatalytic activity. Chem. Eng. J. 221, 222–229.

Xiang, X., Li, F., Huang, Z., 2014. Recent advances in layered double hydroxide-based materials as versatile photocatalysts. Rev. Adv. Sci. Eng. 3, 158–171.

Yao, L., Zhang, Y.C., Li, J., Chen, Y., 2014. Photocatalytic properties of SnS_2/SnO_2 nanocomposite prepared by thermal oxidation of SnS_2 nanoparticles in air. Sep. Purif. Technol. 122, 1–5.

Zhao, X., Zhang, F., Xu, S., Evans, D., Duan, X., 2010. From layered double hydroxides to ZnO-based mixed metal oxides by thermal decomposition: transformation mechanism and UV-blocking properties of the product. Chem. Mater. 22, 3933–3942.

Zhao, X., Wang, L., Xu, X., Lei, X., Xu, S., Zhang, F., 2011. Fabrication and photocatalytic properties of novel $ZnO/ZnAl_2O_4$ nanocomposite with $ZnAl_2O_4$ dispersed inside ZnO network. Mater. Interf. Electrochem. Phen. 58, 573–582.

Zheng, L., Zheng, Y., Chen, C., Zhan, Y., Lin, X., Zheng, Q., Wei, K., Zhu, J., 2009. Network structured SnO_2/ZnO heterojunction nanocatalyst with high photocatalytic activity. Inorg. Chem. 48, 1819–1825.